24. Jones, T. A., Zhou, J. Y., Cowan, S. W. & Kjeldgard, M. Improved methods for building protein models in electron density maps and the location of errors in these models. *Acta Crystallogr. A* **47,** 110–119 (1991).
25. Brunger, A. T. X-PLOR, version 3.85. A system for X-ray diffraction: solvation properties of penicillopepsion and neuraminidase crystal structure. *J. Mol. Biol.* **243,** 100–115 (1994).
26. Jiang, J. S. & Brunger, A. T. Protein hydration observed by X-ray diffraction: solvation properties of penicillopepsion and neuraminidase crystal structure. *J. Mol. Biol.* **243,** 100–115 (1994).
27. Carson, M. Ribbons 2.0. *J. Appl. Crystallogr.* **24,** 958–961 (1991).
28. Nichoos, A. *GRASP: Graphical Representation & Analysis Surface Properties* (Columbia University, New York, 1992).
29. Huang, C. & Mason, J. T. Geometric packing constraints in egg phosphatidylcholine vesicles. *Proc. Natl Acad. Sci. USA* **75,** 308–310 (1978).
30. Vaz, W. L. C., Goodsaid-Zalduondo, F. & Jacobson, K. A. Lateral diffusion of lipids and proteins in bilayer membranes. *FEBS Lett.* **174,** 199–207 (1984).

Acknowledgements. We thank J. Collawn for helpful discussions and critical reading of the manuscript and D. Malehorn for help with site-directed mutagenesis. We thank J. Tsao and Y. Luo for their help in data collection. This work was supported by a grant from the NIH to V.A.B. and NASA to M.L. The X-ray crystallographic coordinates have been deposited in the BNL Protein Data Bank (accession number 1AUA).

Correspondence should be addressed to either V.A.B. (e-mail: vabankaitis@tmg.bhs.uab.edu) or M.L. (e-mail: ming@orion.cmc.vab.edu) and requests for materials should be addressed to M.L.

Energy transduction in ATP synthase

Timothy Elston, Hongyun Wang & George Oster

Department of Molecular and Cellular Biology, University of California, Berkeley, California 94720-3112, USA

Mitochondria, bacteria and chloroplasts use the free energy stored in transmembrane ion gradients to manufacture ATP by the action of ATP synthase. This enzyme consists of two principal domains. The asymmetric membrane-spanning F_o portion contains the proton channel, and the soluble F_1 portion contains three catalytic sites which cooperate in the synthetic reactions[1]. The flow of protons through F_o is thought to generate a torque which is transmitted to F_1 by an asymmetric shaft, the coiled-coil γ-subunit. This acts as a rotating 'cam' within F_1, sequentially releasing ATPs from the three active sites[1–5]. The free-energy difference across the inner membrane of mitochondria and bacteria is sufficient to produce three ATPs per twelve protons passing through the motor. It has been suggested that this protonmotive force biases the rotor's diffusion so that F_o constitutes a rotary motor turning the γ shaft[6]. Here we show that biased diffusion, augmented by electrostatic forces, does indeed generate sufficient torque to account for ATP production. Moreover, the motor's reversibility—supplying torque from ATP hydrolysis in F_1 converts the motor into an efficient proton pump[7]—can also be explained by our model.

Figure 1a shows the molecular geometry of ATP synthase based on the available structural information[5]. Growing evidence indicates that the entire structure of ATPase can be divided into two counter-rotating assemblies (Fig. 1b). We shall call the assembly consisting of a, b, δ and the F_1 hexamer the 'stator', and place our coordinate system on it. The assembly consisting of c, γ and ε is the 'rotor'. Proton flow through the channels at the a–c interface generates torque which drives the rotor and stator in opposite directions. The motor must generate sufficient torque to produce three ATPs per revolution, an amount of work equivalent to $\sim 20\, k_B T$ per ATP molecule (k_B is Boltzmann's constant and T the absolute temperature; at room temperature $1\, k_B T \approx 0.6\,\mathrm{kcal\,mol^{-1}} = 4.1\,\mathrm{pN\,nm}$).

The central proton carrier in F_o is Asp 61, which is found on the c subunit in 9–12 copies[8,9]. Arg 210 is also an essential amino acid, and it resides on the a subunit in a single copy. (His 245 and Glu 219 are also involved, but may not be essential[10].) These residues hold protons in an energy well whose depth is related to their pK_a values by $V/k_B T \approx -2.3\,\mathrm{p}K_a$. The sequence and topological arrangement of the amino acids in the a and c subunits have been determined, although their exact geometric configuration is uncertain[3,5,11]. The charge configuration we show here is the simplest geometry consistent with structural data; however, our mathematical description can accommodate other charge geometries[12,13]. The geometrical relationship of the rotor Asp 61 sites and the stator Arg 210 site is shown in Fig. 2a. The key elements in this structure are: (1) the two half-channels that allow access of protons from the acidic and basic reservoirs to the rotor sites are offset, which confers an asymmetry on the proton flux. The notion of aqueous half-channels was first proposed for the bacterial flagellar motor[14,15]. (2) The location of the positive stator charge between the half-channels is in a position to interact electrostatically with the rotor sites[13].

The pK_a of Arg 210 is high enough that it is always protonated, and so its charge is fixed at +1. The rotor sites, however, have an intermediate pK_a, and so can be either protonated or not. When unprotonated, they cannot rotate out of the rotor–stator interface, for that would entail a large free energy penalty. Thus all rotor sites facing the bilayer must be protonated, and the membrane interface prevents any unprotonated rotor site from moving out the stator.

Arg 210 interacts with the rotor sites according to Coulomb's law in a dielectric and shielding environment typical of a protein interior (Table 1). If a rotor site passes close to the Arg 210 stator charge, the electrostatic interaction can reduce the rotor pK_a allowing the proton to dissociate. (This is because a protonated site is not exactly neutral, but constitutes a dipole whose strength is not sufficient to prevent it rotating into the bilayer but is strong enough to interact with a nearby charge.) The work of reducing a

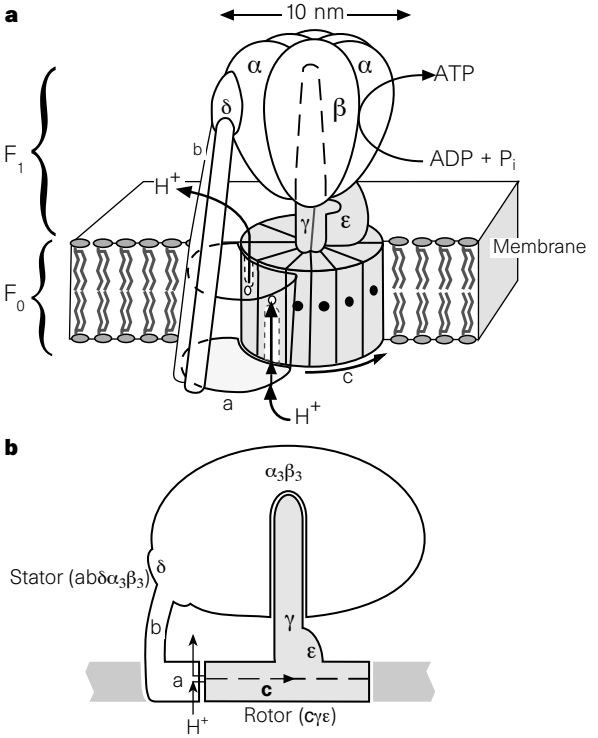

Figure 1 Structure of F_oF_1 ATP synthase[5,6]. **a**, The c subunit consists of 9–12 twin α-helices arranged in a central membrane-spanning array[8]. The a subunit consists of 5–7 membrane-spanning α-helices. The proton channels lie at the interface between the a and c subunits (dashed lines indicate the putative inlet and outlet channels). The a subunit is connected to F_1 by the b and δ subunits. Proton flow through the channels develops torque between the a and c subunits. This torque is transmitted to F_1 via the γ shaft and the ε subunit, where it is used to release ATP sequentially from the three catalytic sites in F_1. (Adapted from refs 4, 5.) **b**, Profile of the F_oF_1 structure showing the two counter-rotating structures. We put our coordinate system on the 'stator', which consists of the a, b, δ subunits and the F_1 hexamer. The 'rotor' is shaded, corresponding to the shaded region in **a**; it comprises the c, γ and ε subunits.

rotor site's pK_a values carries an energetic price: the proximity of a rotor and stator charge creates an electrostatic force between the rotor and stator that impedes its rotation.

The stator charges involved in proton transport are located on adjacent α-helices in the a subunit. Therefore, we shall assume that there are two rotor Asp 61 sites at the rotor/stator interface, as shown in Fig. 2a. We shall also assume that the rotor sites are accessible from the low- and high-pH sides through aqueous channels in the stator[11,14,16]. Protons in the acidic reservoir have access to the right-hand rotor site and protons in the basic reservoir have access to the left-hand rotor site. We place the positively charged Arg 210 stator residue in a position midway between the two aqueous channels, and offset 0.52 nm out of the rotor plane.

Intuitively, the motor works as follows. First consider the situation when the positive stator charge is absent, which has been discussed elsewhere[6]. The two rotor sites within the stator can be protonated or unprotonated. When both sites are unprotonated, the rotor cannot diffuse in either direction, for that would entail moving an Asp 61 site into the bilayer. When the right-hand site is protonated, the rotor can diffuse to the right unimpeded, but is prevented from diffusing to the left by the other unprotonated site. Conversely, when the left site is neutralized by a proton, it can diffuse to the left, but not to the right. When both sites are neutralized, the rotor can diffuse freely in both directions. When the proton electrochemical potential difference across the membrane tends to drive protons upwards with reference to Fig. 2a, the rotor will diffuse preferentially to the right because the right-hand site will be protonated more often than the left-hand site as it faces a higher proton concentration. Thus, on average, protons enter from the acidic reservoir, board the rotor and rotate to the right by one full revolution, then exit to the basic reservoir when they re-enter the stator from the left. However, this is not an efficient motor, for when both sites are occupied, the rotor will be forced backwards by the load torque, allowing protons to leak through to the basic reservoir without performing any work. Indeed, we will show that, without Arg 210, this biased diffusion cannot account for the observed properties of the motor.

Now consider the situation when the stator charge is present. When the right-hand site is protonated, half the time it will diffuse to the right and enter the membrane. This brings a corresponding charge into the stator from the left, where it can exit to the basic reservoir. However, when the rotor diffuses to the left and approaches the stator charge, its pK_a will drop and it will promptly relinquish its proton back to the acidic reservoir. Unprotonated, the bare site is quickly pulled into apposition with the stator charge and held in place against the load torque. However, a thermal fluctuation can carry the site away from the stator charge far enough to reprotonate from the acidic channel, whereupon the site gets another try at diffusing to the right. The same cycle of events takes place at the basic channel, but owing to the proton gradient, the rotor's diffusion is consistently biased to the right. The presence of the positive stator charge prevents back-diffusion of the rotor and couples the proton flux tightly to the rotor motion. This more than compensates for the retarding effect of the electrostatic interaction,

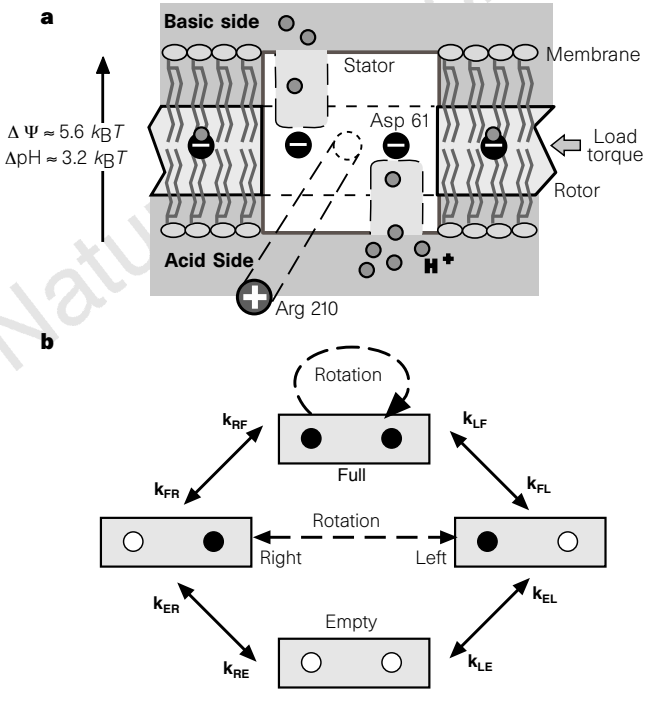

Figure 2 Charge geometry and movement of protons in ATP synthase. **a**, Face-on view showing the relative locations of the stator and rotor charges and the proton channels. The two proton reservoirs are connected by offset 'half-channels' which confer an asymmetry on the assembly[6,14]. Arg 210 is located on the a subunit in a plane 0.52 nm offset from the plane of the rotor. **b**, Markov chain describing the four possible motor states and their transition rates, $k_{i\to j}$. E, empty; F, full; L, left site occupied; R, right site occupied. White circles, unprotonated Asp 61 sites; black circles, protonated sites.

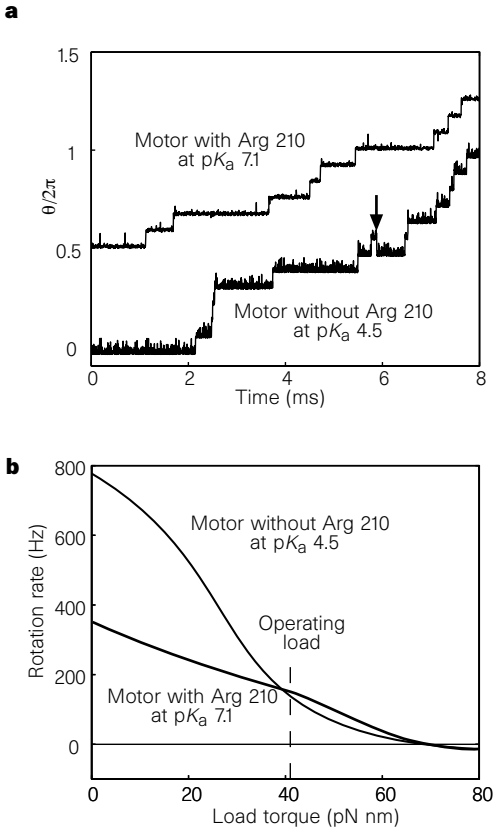

Figure 3 Properties of the ATP synthase rotor. **a**, Stochastic simulation of the rotor motion when a protonmotive force of 220 mV is imposed across the membrane and a load torque of 41 pN nm resists the motion. In the absence of Arg 210, the rotor advances in steps, with occasional reversals (arrow), when protons can leak through the stator without advancing the rotor. When Arg 210 is present, the motor suffers almost no reversals, and the amplitude of its stochastic fluctuation is smaller. **b**, Angular velocity plotted against load torque for the motors with and without Arg 210.

and enables the engine to work more efficiently as both a motor and pump. To justify this qualitative description of the motor's operation, we must write and solve the equations governing the rotor motion. Various aspects of this mechanism have already been discussed qualitatively[4,13,17–19].

Proton motions are much faster than rotation of the rotor. This enables us to model the movements of the protons by transitions between a set of discrete states (that is, a Markov chain[20]). As each site can be protonated or not, there are four possible protonation states of the assembly, denoted by s = R (right), L (left), E (empty), F (full), as in Fig. 2b. Each time a proton hops into or out of the stator, or the rotor moves, the state switches, and in each state the rotor experiences different torques.

We can neglect inertia and describe the rotation of the rotor by a torque balance that includes thermal fluctuations[21]:

$$\underbrace{\zeta 2\pi\Omega(\theta)}_{\text{viscous drag torque}} = \underbrace{F_E(\theta,s)}_{\text{electrostatic torques from the stator}} + \underbrace{F_H(\theta,s)}_{\text{hydrophobic torque from the membrane}} - \underbrace{\tau}_{\text{load torque from } F_1} + \underbrace{f(t)}_{\text{brownian torque}}, s = \mathrm{R, L, E, F} \quad (1)$$

Here $2\pi\Omega = \mathrm{d}\theta(t)/\mathrm{d}t$ is the angular velocity of the rotor, ζ is the drag coefficient of the rotor, τ is the load torque from F_1, and $f(t)$ is the brownian torque from thermal fluctuations. $F_E(\theta,s)$ is the electrostatic torque acting on the rotor from the interaction between rotor charges and Arg 210. The hydrophobic force, F_H, arises from the potential barrier preventing the motion of an unprotonated site into the membrane; this energy barrier is $\sim 45\, k_BT$. To compute the torque generated by the motor, equation (1) must be solved simultaneously with the Markov process governing the hopping of protons on and off of the rotor sites.

The model equations were solved numerically using the parameter values listed in Table 1; the details of all computations are given in Supplementary Information. Figure 3a shows a stochastic simulation of the rotor motion when the proton flow through the stator is driven by a protonmotive force of $\Delta p \sim 220$ mV and the rotor works against a constant load of 41 pN nm, which is equivalent to the torque necessary to produce three ATPs from F_1 per rotation. We see that the motor progresses stepwise, each step corresponding to the passage of one proton through the motor.

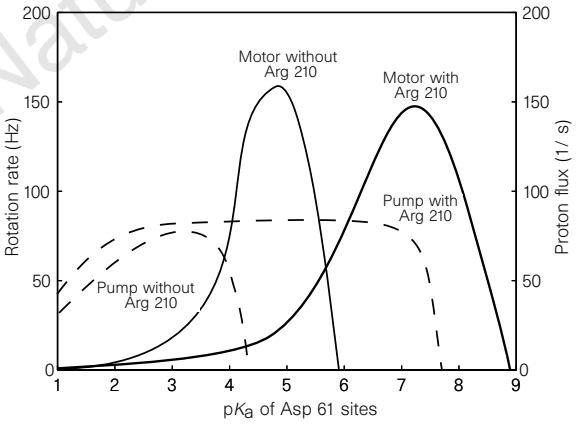

Figure 4 Solid lines show the rotation rate of the motor as a function of the pK_a of the rotor Asp 61 sites with and without the presence of the stator Arg 210 charge when the load torque is fixed at 41 pN nm. The optimum pK_a for the motor operating without Arg 210 is 4.5–5; in the presence of Arg 210, the optimum is 7–7.5. Dashed lines show the reverse proton flux when the motor operates in reverse as a proton pump. $200 k_BT\,s^{-1}$ is supplied by F_1 to rotate the γ-subunit. In the absence of Arg 210, the optimal pK_a is 3–3.5, whereas in the presence of Arg 210, the optimum is 6–7. These plots show that Arg 210 is necessary for F_o to function as both a motor and a pump.

On average, 12 protons pass through the motor per rotation, corresponding to 4 protons per ATP. The rotation is tightly coupled to the proton flux because the presence of Arg 210 prevents leakage of protons by back-rotation. Figure 3b shows a load–velocity curve for the F_o motor. As rotation is tightly coupled with proton flow, the motor efficiency increases roughly in proportion to the load. When rotating against the 'normal' load torque from F_1, the motor is operating at ~60% efficiency. It is likely that the load from F_1 is not constant, so several other load patterns were investigated: our general conclusions were unaltered.

The crucial role of electrostatic forces can be demonstrated quantitatively by computing the motor performance with and without the stator Arg 210 residue. In Fig. 4 we have plotted the rotation rate of the motor as a function of the pK_a of the rotor sites. In the presence of Arg 210, the optimal motor performance is close to the measured pK_a value of 7.1 (ref. 22). In the absence of the stator charge, the motor cannot develop any torque above p$K_a \sim 6$, and is completely decoupled from the proton flux. To work without the stator charge, the rotor pK_a must be lowered to 4.5–5, close to its solution value. In Fig. 3a we have plotted a stochastic simulation of the motor in the absence of Arg 210 at a rotor pK_a of 4.5. It operates quite well, but suffers occasional reversals because it cannot resist the load torque in the doubly occupied F state. Thus without the electrostatic coupling induced by Arg 210, the motor is not as tightly coupled to the proton flux. Moreover, to produce sufficient torque at this low pK_a the entry rate of protons must be at least $10^4\,s^{-1}$, because most protons promptly dissociate back into the acidic reservoir (see Supplementary Information).

There is an additional constraint on the motor's performance. Under anaerobic conditions, the ATP synthase of *Escherichia coli* reverses, using ATP hydrolysis to pump protons against a pH gradient. To investigate the performance of the motor as a pump, we assumed an ATP hydrolysis rate by F_1 of 50 ATP molecules per second[23], an efficiency of 20% in converting this to rotary torque (corresponding to a power input of $2\pi\Omega\tau$), and a gradient of 1 pH unit. The basic reservoir was maintained at a pH of 7.6 as this is the value at which *E. coli* maintains its cytoplasm. Figure 4 shows that, in the absence of Arg 210, the optimal pK_a of the rotor sites is 3–3.5, quite far from the optimal operating region for the motor. Above p$K_a \approx 4.3$, the motor can no longer act as a pump. Thus without Arg 210, the motor is a poor proton pump. However, in the presence of Arg 210, it performs quite well as a proton pump near the optimal pK_a for the motor. Therefore, omitting the electrostatic forces in equation (1) prevents the motor from operating efficiently as both a motor and pump. Moreover, the many protonation–deprotonation

Table 1 Parameter values used in calculations

Parameter	Value
Proton diffusion coefficient (D_p)	9.3×10^9 nm^2 s^{-1}
Rotary diffusion coefficient of the rotor (D_r)	2×10^4 s^{-1}
Dielectric constant of channel (ϵ_c)	10
Dielectric constant of the membrane (ϵ_m)	3
Bilayer viscosity (η)	1 poise
Height of rotor (h)	6 nm
Shielding length of channel charges ($1/\lambda$)	1.1 nm
pH^A (pH of acidic reservoir)	motor, 7; pump, 6.6
pH^B (pH of basic reservoir)	motor, 8.4; pump, 7.6
'Radius' of the proton channel (r)	0.5 nm
Radius of rotor (R)	5 nm
Distance (Δx) between Asp 61 residues, $2\pi R/12$	2.6 nm
pH difference across the rotor (ΔpH)	80 mV $= 3.2 k_BT$
Membrane potential ($\Delta\psi$)	140 mV $= 5.6 k_BT$

events that occur before a successful rotor movement require a high entry rate for protons in order to generate sufficient torque.

The average electrostatic torque felt by the rotor opposes the rotor's motion, so that the field actually works against the motor. However, this energy penalty is more than compensated for by two beneficial effects: (1) the high pK_a of the rotor sites holds protons tightly and prevents futile protonation–deprotonation cycles: this increases the effective proton supply to the stator; (2) by forcing the rotor site to relinquish its proton when passing the stator charge, the stator charge tightly couples the proton flux to the rotor motion. This increases the effectiveness of rectifying the rotor's diffusion, and more than compensates for the additional work done by the protonmotive force against the electric field.

We have presented a mechanism for transducing free energy stored in an ion gradient into a rotary torque. Our analysis delineates the quantitative conditions under which the structure shown in Fig. 1 can actually generate the power required for ATP synthesis. This mechanism has several attractive properties. First, the motor can be reversed to form a proton pump, as in *E. coli* and the V-ATPase proton pumps[24]. Second, the motor works as well when other ions are substituted for protons: for example, the F_oF_1 ATPase of *Progenium modestum*, which is very similar in structure to ATP synthase but operates on sodium ions rather than protons[25]. Finally, the model provides an explanation for the effects of mutations in the crucial rotor and stator amino acids[10]. In addition to elucidating the mechanisms of torque generation, the model provides a framework for integrating the kinetic, thermodynamic and mechanical aspects of protonmotive energy transduction. □

Received 20 August; accepted 27 October 1997.

1. Boyer, P. The binding change mechanism for ATP synthase—some probabilities and possibilities. *Biochim. Biophys. Acta* **1140,** 215–250 (1993).
2. Abrahams, J., Leslie, A., Lutter, R. & Walker, J. Structure at 2.8 Å resolution of F_1-ATPase from bovine heart mitochondria. *Nature* **370,** 621–628 (1994).
3. Fillingame, R. H. Coupling H^+ transport and ATP synthesis in F_1F_o-ATP synthases: glimpses of interacting parts in a dynamic molecular machine. *J. Exp. Biol.* **200,** 217–224 (1997).
4. Cross, R. & Duncan, T. Subunit rotation in F_oF_1-ATP synthases as a means of coupling proton transport through F_o to the binding changes in F_1. *J. Bioenerg. Biomem.* **28,** 403–408 (1996).
5. Engelbrecht, S. & Junge, W. ATP synthase: a tentative structural model. *FEBS Lett.* **414,** 485–491 (1997).
6. Junge, W., Lill, H. & Engelbrecht, S. ATP synthase: An electro-chemical transducer with rotatory mechanics. *Trends Biochem. Sci.* **22,** 420–423 (1997).
7. Yasuda, R., Noji, H., Kinosita, K., Motojima, F. & Yoshida, M. Rotation of the γ subunit in F_1-ATPase; Evidence that ATP synthase is a rotary motor enzyme. *J. Bioenerg. Biomem.* **29,** 207–209 (1997).
8. Groth, G. & Walker, J. Model of the C-subunit oligomer in the membrane domain of F-ATPases. *FEBS Lett.* **410,** 117–123 (1997).
9. Dmitriev, O. Y., Altendorf, K. & Fillingame, R. H. Reconstitution of the F_o complex of *Escherichia coli* ATP synthase from isolated subunits: Varying the number of essential carboxylates by co-incorporation of wild-type and mutant subunit c after purification in organic solvent. *Eur. J. Biochem.* **233,** 478–483 (1995).
10. Valiyaveetil, F. & Fillingame, R. On the role of Arg 210 and Glu 219 of subunit a in proton translocation by the *Escherichia coli* F_oF_1 ATP synthase. *J. Biol. Chem.* (in the press).
11. Fillingame, R. H., Girvin, M. E. & Zhang, Y. Correlations of structure and function in subunit c of *Escherichia coli* F_oF_1 ATP synthase. *Biochem. Soc. Trans.* **23,** 760–766 (1995).
12. Howitt, S., Rodgers, A., Hatch, L., Gibson, F. & Cox, G. The coupling of the relative movement of the a and c subunits of the F_o to the conformational changes in the F1-ATPase. *J. Bioenerg. Biomem.* **28,** 415–420 (1996).
13. Vik, S. B. & Antonio, B. J. A mechanism of proton translocation by F_1F_o ATP synthases suggested by double mutants of the a subunit. *J. Biol. Chem.* **269,** 30364–30369 (1994).
14. Khan, S. & Berg, H. Isotope and thermal effects in chemiosmotic coupling to the flagellar motor of *Streptococcus. Cell* **32,** 913–919 (1983).
15. Meister, M., Caplan, S. R. & Berg, H. C. Dynamics of a tightly coupled mechanism for flagellar rotation: Bacterial motility, chemiosmotic coupling, protonmotive force. *Biophys. J.* **55,** 905–914 (1989).
16. Berg, H. & Khan, S. in *Mobility and Recognition in Cell Biology* (eds Sund, H. & Veeger, C.) 485–497 (de Gruyter, Berlin, 1983).
17. Sabbert, D., Engelbrecht, S. & Junge, W. Intersubunit rotation in active F-ATPase. *Nature* **381,** 623–625 (1996).
18. Fillingame, R. in *The Bacteria: A Treatise On Structure And Function* (ed. Krulwich, T.) 345–392 (Academic, London, 1990).
19. Harrison, M., Finbow, M. & Findlay, J. Postulate for the molecular mechanism of the vacuolar H^+-ATPase (hypothesis). *J. Membr. Biol.* **14,** 1–3 (1997).
20. Elston, T. & Oster, G. Protein turbines I: The bacterial flagellar motor. *Biophys. J.* **73,** 703–721 (1997).
21. Risken, H. *The Fokker-Planck Equation* (Springer, New York, 1989).
22. Assadi-Porter, F. & Fillingame, R. Proton-translocating carboxyl of subunit c of $F_1F_oH^+$-ATP synthase: The unique environment suggested by the pKa determined by ^{1}H NMR. *Biochem.* **34,** 16186–16193 (1995).
23. Noji, H., Yasuda, R., Yoshida, M. & Kinosita, K. Direct observation of the rotation of F_1-ATPase. *Nature* **386,** 299–302 (1997).
24. Finbow, M. & Harrison, M. The vacuolar H^+-ATPase: A universal proton pump of eukaryotes. *Biochem. J.* **324,** 697–712 (1997).
25. Dimroth, P. Primary sodium ion translocating enzymes. *Biochim. Biophys. Acta* **1318,** 11–51 (1997).

Supplementary information is available on *Nature*'s World-Wide Web site (http://www.nature.com) or as paper copy from Mary Sheehan at the London editorial office of *Nature*.

Acknowledgements. We thank C. Peskin, R. Fillingame, W. Junge, H.-P. Moore, J. Walker, R. Cross, and S. Khan for valuable comments. T.E. was suppported by postdoctoral support from Los Alamos National Laboratory, H.W. by a postdoctoral fellowship from National Energy Research Scientific Computing Center, and G.O. by a grant from the NSF.

Correspondence and requests for materials should be addressed to G.O. (e-mail: goster@nature.berkeley.edu).

(a)

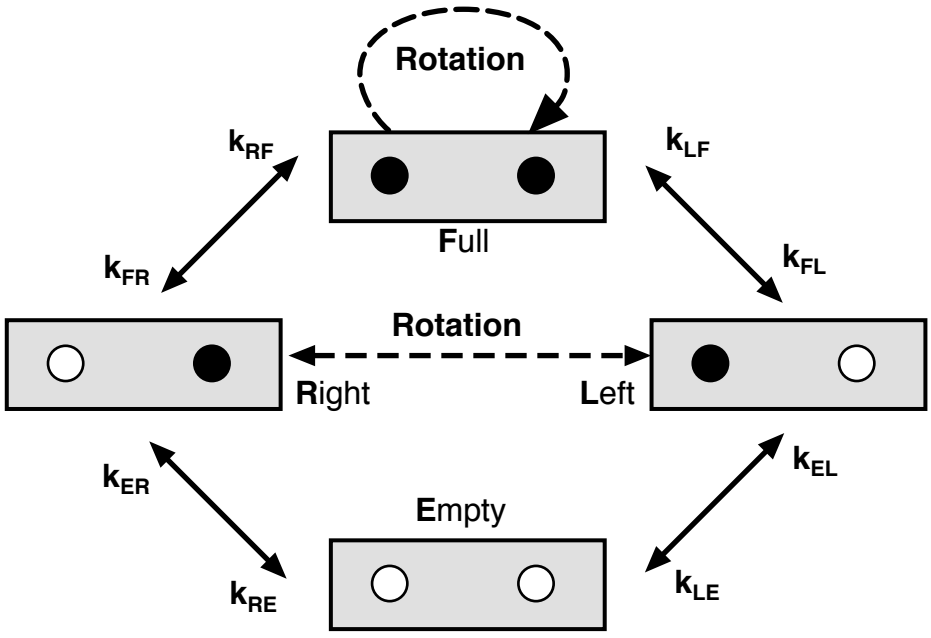

(b)

Elston et al.
Figure 2 a,b

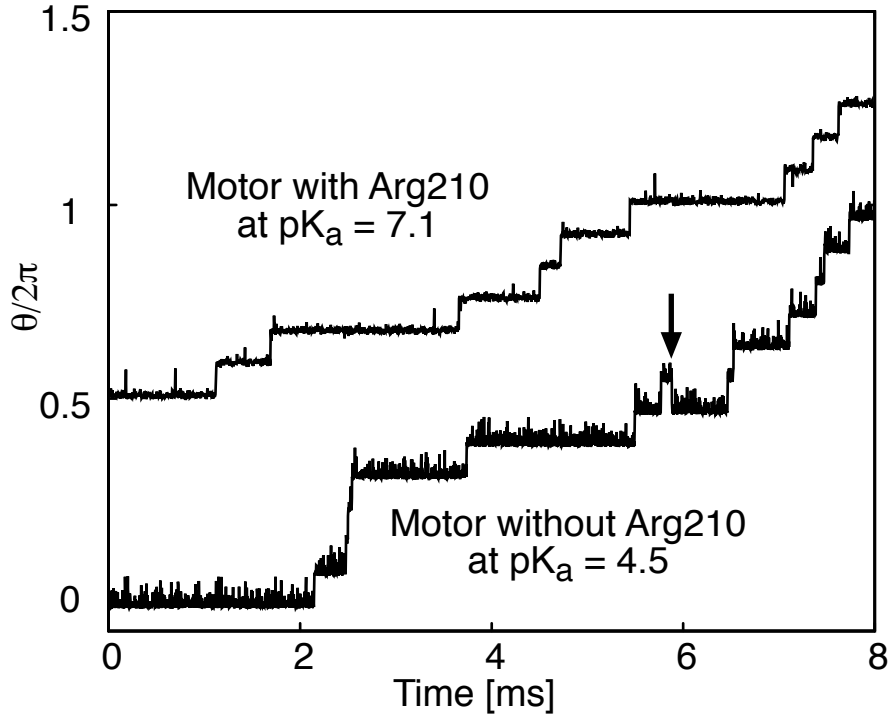

(**a**)

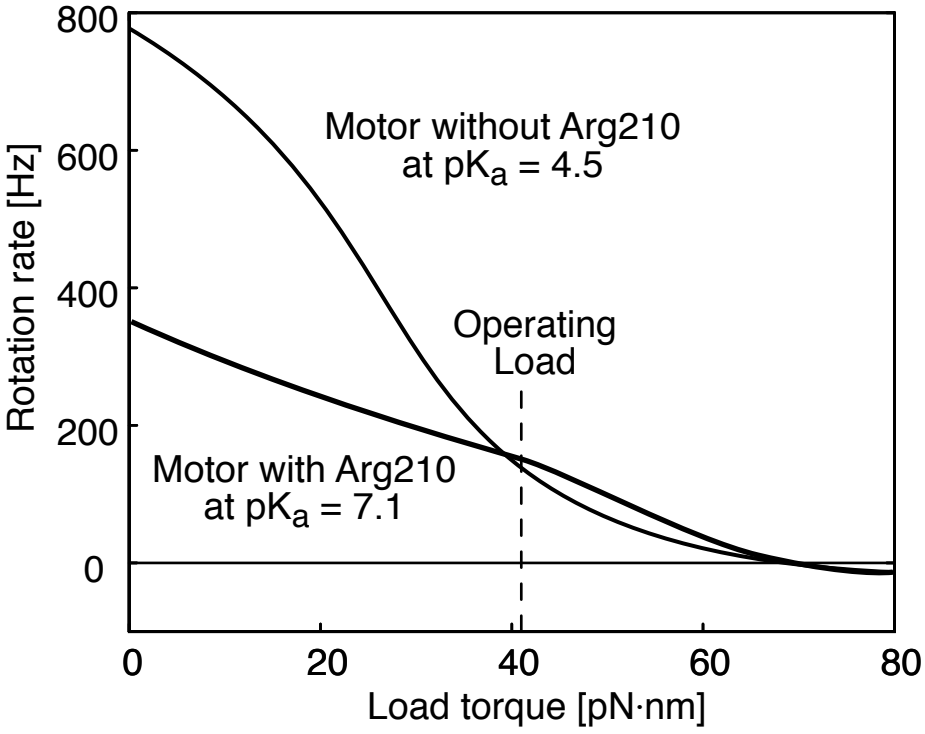

(**b**)

Elston et al.
Figure 3 a,b

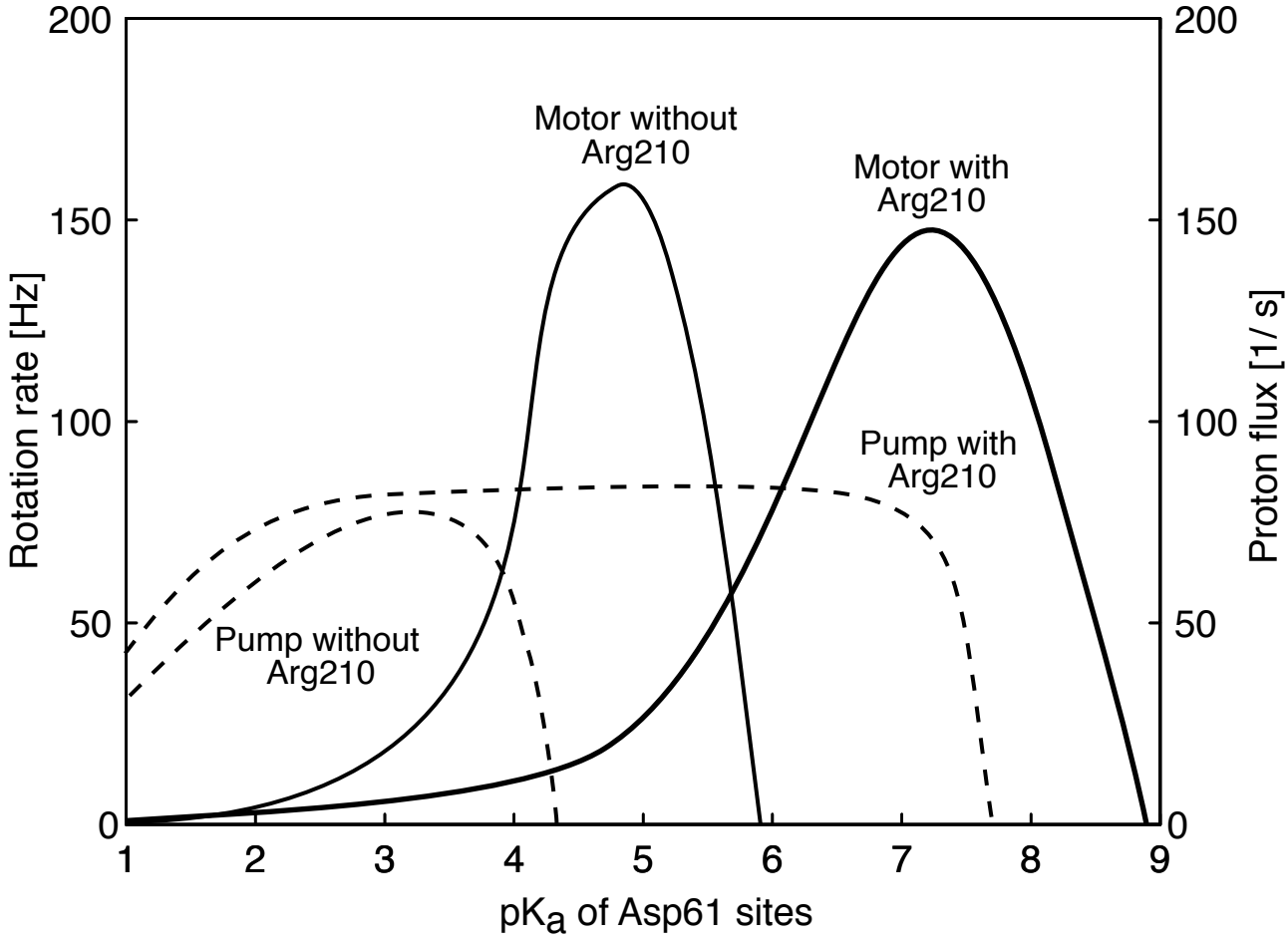

Elston et al.
Figure 4

Mathematical formulation of the F_0 motor model

A. Markov chain model for the evolution of the rotor state

The four possible protonation states of the two rotor Asp61 sites at the rotor-stator interface are:

Both sites empty (**E**) :	(o o)
The right site protonated (**R**) :	(o •)
Both sites protonated (**F**) :	(• •)
The left site protonated (**L**) :	(• o)

As protons hop into and out of the channel, the state of the two exposed rotor sites changes. Figure 1 shows the transitions between these rotor states due to proton hops. The Markov transition matrix corresponding to the transition diagram in Figure 1 is:

$$\mathbf{K} = \begin{bmatrix} -(k_{ER}+k_{EL}) & k_{RE} & 0 & k_{LE} \\ k_{ER} & -(k_{RE}+k_{RF}) & k_{FR} & 0 \\ 0 & k_{RF} & -(k_{FR}+k_{FL}) & k_{LF} \\ k_{EL} & 0 & k_{FL} & -(k_{LE}+k_{LF}) \end{bmatrix} \tag{1}$$

We assume that protons cannot hop between the Asp61 sites. At any fixed rotor position, it takes two proton hops to go from state **R** (o •) to state **L** (• o) (i.e. one proton hops out and another one hops in). So there is no direct Markov transition between **R** and **L** in Figure 1. However the transition between **R** and **L** can be done by a rotation of the rotor (shown as dashed line in Figure 1). For example, when the rotor is in state **R** (o •), a rotation to the right can push the protonated site on the right into the membrane and pull a protonated site out of the membrane on the left, which changes the rotor into state **L** (• o).

In Figure 2, we plot the free energy change, $\Delta G(\theta, \mathbf{s})$, in the system as a function of rotation angle, θ, and rotor state, **s**, when one proton passes through the motor producing a rotation of $2\pi/12$ radian against a load torque of 41 pN-nm. The cycle shown is the power cycle $\mathbf{E} \rightarrow \mathbf{R} \rightarrow \mathbf{L} \rightarrow \mathbf{E}$. The protonmotive force across the membrane is Δp = 220 mV (= 8.8 k_BT). The work done by the proton against the load torque is 41 pN-nm x $(2\pi/12)$ = 5.2 k_BT. The energy dissipated in the process is 8.8 – 5.2 = 3.6 k_BT. In Figure 2, the free energy curve for state **E** at the end of the cycle is 3.6 k_BT lower than the one for state **E** at the beginning of the cycle.

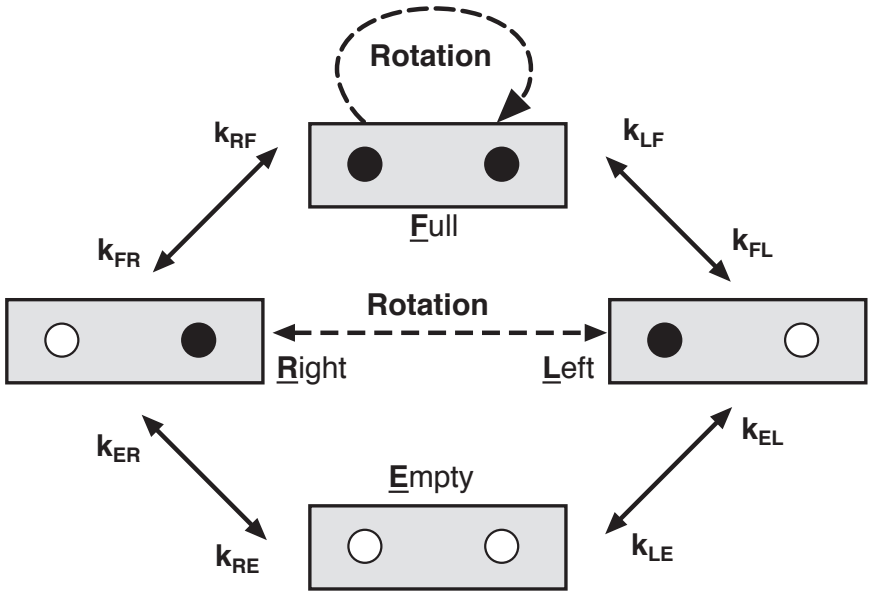

Figure 1 Markov chain describing the four possible rotor states and their transition rates, $k_{i\rightarrow j}$. **E** = Empty, **F** = Full, **L** = Left site occupied, **R** = Right site occupied. (o) = unprotonated Asp61 sites, (•) = protonated sites.

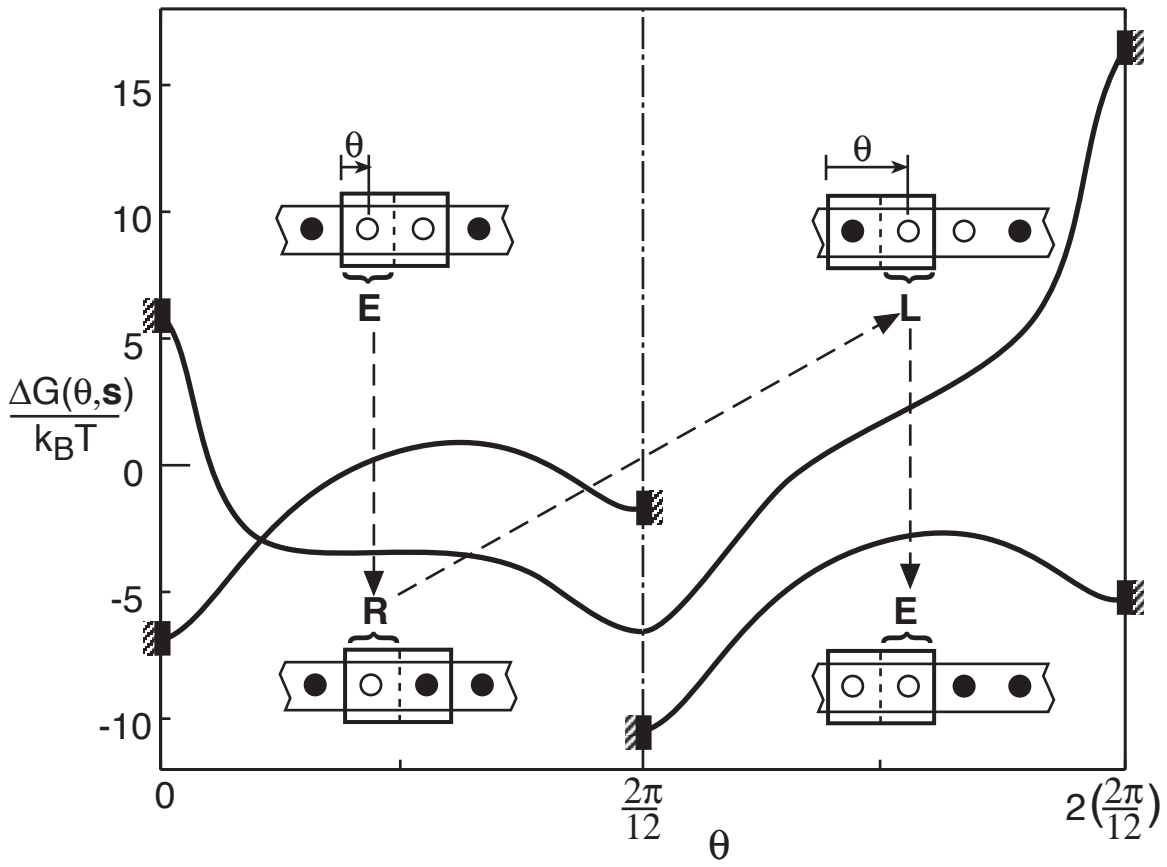

Figure 2 Free energy change, $\Delta G(\theta, \mathbf{s})$, in the system as a function of rotation angle, θ, and rotor state, **s**, when one proton passes through the motor producing a rotation of $2\pi/12$ radian against a load torque of 41 pN-nm. The reflecting membrane boundaries are denoted by solid rectangles. The cycle shown is the power cycle $\mathbf{E} \rightarrow \mathbf{R} \rightarrow \mathbf{L} \rightarrow \mathbf{E}$; other cycles shown in Figure 1 are not power producing, and involve rotor slip and/or proton leakage. The protonmotive force across the membrane is $\Delta p = 220$ mV $\approx 8.8\ k_BT$. The work done by the proton against the load torque is 41 pN-nm x $(2\pi/12) = 5.2\ k_BT$. The energy dissipated in the process is $8.8 - 5.2 = 3.6\ k_BT$, so the free energy curve for state **E** at the end of the cycle is $3.6\ k_BT$ lower than the one for state **E** at the beginning of the cycle.

B. Langevin equation formulation

Since inertia is negligible, equating the viscous drag on the rotor to the forces acting on it yields the Langevin equation [1, 2]

$$\zeta \frac{d\theta}{dt} = -\frac{d\psi_E(\theta;s)}{d\theta} - \frac{d\phi_H(\theta;s)}{d\theta} - \tau + f(t), \qquad \mathbf{s} = \mathbf{L}, \mathbf{R}, \mathbf{E}, \mathbf{F} \tag{2}$$

where:

- ζ = drag coefficient of the c-rotor.
- $f(t)$ = the random force due to brownian fluctuations. The brownian force is modeled in the usual way by a Gaussian distribution with unit mean and amplitude $\sqrt{2\zeta k_B T \Delta t}$, where Δt is the time step in the numerical simulation [2].
- τ = load torque from F_1.
- **s** = (**E**, **R**, **F**, **L**). The state of the two exposed rotor sites evolves according to the transition rates k_{ij} shown in Figure 1.
- $\psi_E(\theta; \mathbf{s})$ = the potential affecting the rotor in state **s**. $\psi_E(\theta; \mathbf{s})$ contains the interactions between the rotor sites and the fixed stator charges (Arg210, Glu219, and His245).
- $\phi_H(\theta; \mathbf{s})$ = the hydrophobic potential barrier preventing the rotation of unprotonated rotor sites into the membrane. The energy barrier against rotating an unprotonated Asp61 site into the bilayer depends on the difference in the dielectric constants between the two media: $\Delta G \approx 200\left(\frac{1}{\varepsilon_{membrane}} - \frac{1}{\varepsilon_{stator}}\right)$ [3]. Taking $\varepsilon_{mem} \approx 3$ and $\varepsilon_{stator} \approx 10$, we have $\Delta G \approx 45\ k_BT$.

Note that $\psi_E(\theta; \mathbf{s})$ and $\phi_H(\theta; \mathbf{s})$ could be combined into one potential in equation (2). However, we keep them separate because in the Fokker-Planck formulation, the effect of the membrane potential barrier, $\phi_H(\theta; \mathbf{s})$, is modeled by boundary conditions, while

the effect of rotor-stator charge interactions are carried by the potential $\psi(\theta; \mathbf{s})$, which resides in the equations of motion.

To compute the torque generated by the motor, equations (2) must be solved simultaneously with the Markov process governing the hopping of protons on and off of the rotor sites. Although we draw the rotation of the rotor as a link (dashed line) between states **R** and **L**, the rotation of the rotor from θ to $\theta+2\pi/12$ cannot be treated simply as a single Markov step for the reasons listed below:

- The rotation of the rotor is continuous. The rotation of the rotor from θ to $\theta+\delta$ can be treated as a single Markov step only if the diffusion of the rotor in $[\theta, \theta+\delta]$ is much faster than the net rotation of the rotor from θ to $\theta+\delta$. The time scale for diffusion in $[\theta, \theta+\delta]$ is $\sim\delta^2/D$ and the time scale of the net rotation is $\sim\delta/\langle v\rangle$. Therefore, if δ is small enough, the diffusion is always faster than the net rotation. This is the essence of the numerical discretization of the model. However, $\delta = 2\pi/12$ is not small enough, so the rotation from θ to $\theta+2\pi/12$ cannot be treated as a single Markov step; instead it has to be treated as a sequence of smaller Markov steps.
- The effect of the stator charge, Arg210, on the rotor is strongly angle-dependent. When a protonated rotor site passes Arg210, the stator charge reduces the effective pK_a of the rotor site and forces the rotor site to relinquish its proton. When a rotor site is far from the stator charge, its large pK_a can hold the proton tightly. This prevents many futile protonation and deprotonation cycles. If we treat the rotation from θ to $\theta+2\pi/12$ as a single Markov step, then we cannot model the angle-dependence of the interactions between the stator and rotor charges.

C. Fokker-Planck equation formulation

In the Fokker-Planck formulation corresponding to equations (2), the state of the system is described by the four probability density functions:

$$\boldsymbol{\rho}(\theta,t) = \begin{bmatrix} \rho_E(\theta,t) \\ \rho_R(\theta,t) \\ \rho_F(\theta,t) \\ \rho_L(\theta,t) \end{bmatrix} \tag{3}$$

where $\rho_s(\theta,t)$ is the probability density that the motor is in state **s** and the rotor is at location θ at time t. These distributions evolve according to the convective diffusion equations

$$\frac{\partial \boldsymbol{\rho}}{\partial t} = \frac{1}{\zeta_r}\frac{\partial}{\partial\theta}\left\{\left(\frac{d\boldsymbol{\Psi}}{d\theta}+\tau\right)\boldsymbol{\rho}\right\} + D_r\frac{\partial^2\boldsymbol{\rho}}{\partial\theta^2} + \mathbf{K}\boldsymbol{\rho} \tag{4}$$

where $D_r = k_B T/\zeta_r$ is the diffusion coefficient of the c-rotor. The electrostatic potential matrix is

$$\mathbf{\Psi}(\theta) = \begin{bmatrix} \psi_E(\theta) & 0 & 0 & 0 \\ 0 & \psi_R(\theta) & 0 & 0 \\ 0 & 0 & \psi_F(\theta) & 0 \\ 0 & 0 & 0 & \psi_L(\theta) \end{bmatrix} \tag{5}$$

where $\psi_s(\theta)$ is the potential acting on the rotor due to the electrostatic interactions between the rotor sites and the stator charges when the two rotor sites are in state **s**.

The boundary conditions for equation (4) are given by

- Boundary condition for ρ_E ((o o): reflecting at $\theta = 0$ and at $\delta = 2\pi/12$):

$$\left\{\frac{1}{\zeta}\left(\frac{d\psi_E}{d\theta} + \tau\right)\rho_E + D\frac{\partial \rho_E}{\partial \theta}\right\}_{\theta=0} = 0\,; \quad \left\{\frac{1}{\zeta}\left(\frac{d\psi_E}{d\theta} + \tau\right)\rho_E + D\frac{\partial \rho_E}{\partial \theta}\right\}_{\theta=\delta} = 0 \tag{6}$$

- Boundary condition for ρ_R ((o •): reflecting at $\theta = 0$):

$$\left\{\frac{1}{\zeta}\left(\frac{d\psi_R}{d\theta} + \tau\right)\rho_R + D\frac{\partial \rho_R}{\partial \theta}\right\}_{\theta=0} = 0 \tag{7}$$

- Boundary condition for ρ_F ((• •): periodic with period = δ):

$$\left\{\frac{1}{\zeta}\left(\frac{d\psi_F}{d\theta} + \tau\right)\rho_F + D\frac{\partial \rho_F}{\partial \theta}\right\}_{\theta=0} = \left\{\frac{1}{\zeta}\left(\frac{d\psi_F}{d\theta} + \tau\right)\rho_F + D\frac{\partial \rho_F}{\partial \theta}\right\}_{\theta=\delta} \tag{8}$$

- Boundary condition for ρ_L ((• o): reflecting at $\theta = \delta$):

$$\left\{\frac{1}{\zeta}\left(\frac{d\psi_L}{d\theta} + \tau\right)\rho_L + D\frac{\partial \rho_L}{\partial \theta}\right\}_{\theta=\delta} = 0 \tag{9}$$

- The probability flux leaving the right end ($\theta = \delta$) of state **R** is equal to the flux entering the left end ($\theta = 0$) of state **L**:

$$\left\{\frac{1}{\zeta}\left(\frac{d\psi_R}{d\theta} + \tau\right)\rho_R + D\frac{\partial \rho_R}{\partial \theta}\right\}_{\theta=\delta} = \left\{\frac{1}{\zeta}\left(\frac{d\psi_L}{d\theta} + \tau\right)\rho_L + D\frac{\partial \rho_L}{\partial \theta}\right\}_{\theta=0} \tag{10}$$

D. Numerical Calculations

D.1 Motor without Arg210: A pure Brownian ratchet

In this model, we assume:

- k^A_{in} = the rate of proton hopping into the channel from the acidic side (low pH) of the membrane. It is independent of the rotor position, θ, and independent of the state of the other site.

- k^{B}_{in} = the rate of proton hopping into the channel from the basic side (high pH) of the membrane. It is independent of the rotor position, θ, and independent of the state of the other site.
- k^{A}_{out} = the rate of proton hopping off the site to the acidic side. It is independent of the rotor position, θ, and independent of the state of the other site.
- k^{B}_{out} = the rate of proton hopping off the site to the basic side. It is independent of the rotor position, θ, and independent of the state of the other site.

These transition rates depend on the parameters listed below:

- pH^{A} = proton concentration on the acidic side (low pH) of the membrane.
- pH^{B} = proton concentration on the basic side (high pH) of the membrane.
- $\Delta\psi$ = potential drop across the membrane.
- $\Delta\phi^{A}$ = the potential drop at surface (due to surface charges) at the acidic side of the membrane.
- $\Delta\phi^{B}$ = the potential drop at surface (due to surface charges) at the basic side of the membrane.
- D_p = proton diffusion coefficient.
- r = radius of the channel leading to the rotor sites.

D.2 Transition rates for ratchet model

In this subsection we first use k^{A}_{in} and k^{A}_{out} as an example to demonstrate our step-by-step procedure for calculating the transition rates. Then we give the rate formulas for the model without Arg210.

The reaction on the rotor sites is represented by

$$\mathrm{Asp61^{-}} + \mathrm{H^{+}} \leftrightarrow \mathrm{Asp61 \cdot H}$$

At equilibrium,

$$k_{in} \cdot [\mathrm{Asp61^{-}}] = k_{out} \cdot [\mathrm{Asp61 \cdot H}] \tag{11}$$

By definition, $pK_a = pH + \log_{10} \frac{[\mathrm{Asp61 \cdot H}]}{[\mathrm{Asp61^{-}}]}$, from which

$$\frac{[\mathrm{Asp61 \cdot H}]}{[\mathrm{Asp61^{-}}]} = 10^{pK_a - pH} \tag{12}$$

The proton hopping rates, k_{in} and k_{out}, are related to pK_a by combining (11) and (12):

$$\frac{k_{in}}{k_{out}} = 10^{pK_a - pH}$$

First consider the case where the potential drop across the membrane is zero and there is no surface charge on the membrane. For the acidic reservoir we have

$$\frac{k^A_{in}(0)}{k^A_{out}(0)} = 10^{pK_a - pH^A} \tag{13}$$

The rate $k^A_{in}(0)$ is limited by the rate protons can jump into the channel. We compute the proton rate constants for entry into the channels by the Smoluchowski formula [4]:

$$k_{in} = \begin{pmatrix} \text{surface proton} \\ \text{concentration} \end{pmatrix} \cdot \begin{pmatrix} \text{absorption rate to a perfectly} \\ \text{absorbing disk of radius r} \end{pmatrix} \tag{14}$$

The rate $k^A_{in}(0)$ is given by♦

$$k^A_{in}(0) = \underbrace{0.6\,\text{nm}^{-3} \cdot 10^{-pH^A}}_{\substack{\text{proton concentration} \\ \text{at the acidic side}}} \cdot \underbrace{4\,r \cdot D_p}_{\substack{\text{absorption} \\ \text{rate}}} \tag{15}$$

From equation (13), the rate $k^A_{out}(0)$ is given by

$$k^A_{out}(0) = 0.6\,\text{nm}^{-3} \cdot 10^{-pK_a} \cdot 4\,r \cdot D_p \tag{16}$$

Using the parameter values listed in **Table 1** ($pH^A = 7$, r = 0.5 nm and $D_p = 9.3\text{x}10^9 \text{nm}^2/\text{s}$), we have $k^A_{in}(0) = 1.1\text{x}10^3/\text{s}$. This is the rate of protons hopping into the channel from the acidic side when no surface charge is on the membrane. This proton in-rate is too small to achieve the ATP synthesis rate of 400 ATP/s. The proton in-rate can be increased by increasing the proton concentration near the membrane surface.

The surface charges on the membrane increase (or decrease) the surface concentration of protons, and change the potential drop inside the membrane. The potential drop inside the membrane is the sum of the contribution from membrane potential and the contribution from the surface charges on the membrane. The potential drop inside the membrane is

$$\Delta\psi - \left(\Delta\phi^A - \Delta\phi^B\right) \tag{17}$$

If there is equal amount of surface charges on each side (i.e., $\Delta\phi^A = \Delta\phi^B$), the contribution of the surface charges is zero. The potential drop inside the membrane does not affect the rate of protons jumping into the channel. It only changes the rate

---

♦ 10^{-pH} is the proton concentration in mole/liter. 1 mole/liter = 0.6 molec / nm^3

of protons jumping off the site. So the in-rate and the off-rate for the model without Arg210 are given by

$$k_{in}^{A} = 0.6\,nm^{-3} \cdot 10^{-pH^{A}} \cdot 4r \cdot D_p \cdot \exp\left(\frac{\Delta\phi^{A}}{k_B T}\right) \tag{18}$$

$$k_{out}^{A} = 0.6\,nm^{-3} \cdot 10^{-pK_a} \cdot 4r \cdot D_p \cdot \exp\left(\frac{\left(\Delta\phi^{A} - \Delta\phi^{B}\right) - \Delta\psi}{2k_B T}\right) \tag{19}$$

$$k_{in}^{B} = 0.6\,nm^{-3} \cdot 10^{-pH^{B}} \cdot 4r \cdot D_p \cdot \exp\left(\frac{\Delta\phi^{B}}{k_B T}\right) \tag{20}$$

$$k_{out}^{B} = 0.6\,nm^{-3} \cdot 10^{-pK_a} \cdot 4r \cdot D_p \cdot \exp\left(\frac{\Delta\psi - \left(\Delta\phi^{A} - \Delta\phi^{B}\right)}{2k_B T}\right) \tag{21}$$

For the model without Arg210, the transition matrix entries are given by

$$\begin{aligned} k_{ER} &= k_{LF} = k_{in}^{A} \\ k_{RE} &= k_{FL} = k_{out}^{A} \\ k_{EL} &= k_{RF} = k_{in}^{B} \\ k_{LE} &= k_{FR} = k_{out}^{B} \end{aligned} \tag{22}$$

D.3 Motor including Arg210: Electrostatically assisted ratchet

The transition rates for the model with Arg210 are given by

$$k_{ER}(\theta) = 0.6\,nm^{-3} \cdot 10^{-pH^{A}} \cdot 4r \cdot D_p \cdot \exp\left(\frac{\Delta\phi^{A}}{k_B T}\right) \tag{23}$$

$$k_{RE}(\theta) = 0.6\,nm^{-3} \cdot 10^{-pK_a} \cdot 4r \cdot D_p \cdot \exp\left(\frac{\left(\Delta\phi^{A} - \Delta\phi^{B}\right) - \Delta\psi}{2k_B T}\right) \cdot \exp\left(\frac{\psi_R(\theta) - \psi_E(\theta)}{k_B T}\right) \tag{24}$$

$$k_{EL}(\theta) = 0.6\,nm^{-3} \cdot 10^{-pH^{B}} \cdot 4r \cdot D_p \cdot \exp\left(\frac{\Delta\phi^{B}}{k_B T}\right) \tag{25}$$

$$k_{LE}(\theta) = 0.6\,nm^{-3} \cdot 10^{-pK_a} \cdot 4r \cdot D_p \cdot \exp\left(\frac{\Delta\psi - \left(\Delta\phi^{A} - \Delta\phi^{B}\right)}{2k_B T}\right) \cdot \exp\left(\frac{\psi_L(\theta) - \psi_E(\theta)}{k_B T}\right) \tag{26}$$

$$k_{LF}(\theta) = 0.6\,nm^{-3} \cdot 10^{-pH^{A}} \cdot 4r \cdot D_p \cdot \exp\left(\frac{\Delta\phi^{A}}{k_B T}\right) \tag{27}$$

$$k_{FL}(\theta) = 0.6\,nm^{-3} \cdot 10^{-pK_a} \cdot 4r \cdot D_p \cdot \exp\left(\frac{\left(\Delta\phi^{A} - \Delta\phi^{B}\right) - \Delta\psi}{2k_B T}\right) \cdot \exp\left(\frac{\psi_F(\theta) - \psi_L(\theta)}{k_B T}\right) \tag{28}$$

$$k_{RF}(\theta) = 0.6\,nm^{-3} \cdot 10^{-pH^B} \cdot 4r \cdot D_p \cdot \exp\left(\frac{\Delta\phi^B}{k_B T}\right) \tag{29}$$

$$k_{FR}(\theta) = 0.6\,nm^{-3} \cdot 10^{-pK_a} \cdot 4r \cdot D_p \cdot \exp\left(\frac{\Delta\psi - \left(\Delta\phi^A - \Delta\phi^B\right)}{2k_B T}\right) \cdot \exp\left(\frac{\psi_F(\theta) - \psi_R(\theta)}{k_B T}\right) \tag{30}$$

E. The electrostatic forces act against the rotor motion

The average torque generated directly by the electrostatic interactions between the rotor and stator can be computed from

$$\left\langle \tau_{Electrostatic} \right\rangle = \sum_{S=\mathbf{E},\mathbf{L},\mathbf{R},\mathbf{F}} \int_0^{\frac{2\pi}{12}} \rho_S(\theta) \cdot \left[-\psi_S'(\theta)\right] d\theta \tag{31}$$

At the operating point for ATP synthesis, the average torque generated directly by the electrostatic interactions between the rotor and stator is negative. However this is more than compensated by the effect of the electrostatic interactions on the rotor sites' pK_a's, which tightly couples the proton flux to the rotor motion, and increase the effectiveness of rectifying the rotor's diffusion.

Table 1 lists the parameter values used in the numerical simulations.

The complete simulation code in Matlab™ 5 is available on request.

PARAMETER	Value	
D_p = proton diffusion coefficient	9.3×10^9 nm^2/s	
D_r = rotary diffusion coefficient of the rotor	2×10^4/s *	
ε_c = dielectric constant of channel	10	
ε_m = dielectric constant of the membrane	3	
η = bilayer viscosity	1 poise	
h = height of the rotor	6 nm	
$1/\lambda$ = shielding length of stator charges	1.1 nm	
pH^A = bulk pH of the acidic reservoir	motor = 7	pump = 6.6
pH^B = bulk pH of the basic reservoir	motor = 8.4	pump = 7.6
r = 'radius' of the proton channel	0.5 nm	
R = radius of rotor	5 nm	
Δx = distance between Asp61 residues = $2\pi R/12$	2.6 nm	
ΔpH = pH difference across the membrane	80 mV = 3.2 k_BT	
$\Delta\psi$ = membrane potential	140 mV = 5.6 k_BT	
$\Delta\phi^A$ = potential drop by surface charges at the acidic side	2.3 k_BT (without Arg210) ♦ 2.0 k_BT (with Arg210)	
$\Delta\phi^B$ = potential drop by surface charges at the basic side	2.3 k_BT (without Arg210) ♦ 2.0 k_BT (with Arg210)	

Table 1. Parameter values.

* The diffusion coefficient of the rotor was computed from $D_r = k_BT/(6\pi\eta hR^2)$, and was modified to reflect the fact that part of the rotor is not subject to the membrane viscosity.

♦ Potential drop of 2.3 k_BT by surface charges can reduce the surface pH value (increase the surface concentration) by 1.

References

1. Risken, H. *The Fokker-Planck Equation* (Springer-Verlag, New York, 1989).

2. Doering, C. in *1990 Lectures in Complex Systems* (eds. Nadel, L. & Stein, D.) 3-51 (Addison-Wesley, Redwood City, CA, 1990).

3. Israelachvili, J. *Intermolecular and Surface Forces* (Academic Press, New York, 1992).

4. Berg, H. *Random Walks in Biology* (Princeton University Press, Princeton, N.J., 1983).